Antiferromagnetic-Metal/Ferromagnetic-Metal Periodic Multilayers for On-Chip Thermoelectric Generation

Y.Z. Wang,[1,2] X.M. Luo,[1] Y. Zhang,[1] C. Fang,[1] M.K. Zhao,[1] W.Q. He,[1] G.Q. Yu,[1,3] C.H. Wan,[1,3,*] and X.F. Han[1,2,3,†]

[1] *Beijing National Laboratory for Condensed Matter Physics, Institute of Physics, University of Chinese Academy of Sciences, Chinese Academy of Sciences, Beijing 100190, China*

[2] *Center of Materials Science and Optoelectronics Engineering, University of Chinese Academy of Sciences, Beijing 100049, China*

[3] *Songshan Lake Materials Laboratory, Dongguan, Guangdong 523808, China*

(Received 18 October 2021; revised 23 January 2022; accepted 25 January 2022; published 28 February 2022)

On-chip thermoelectric generation is of vital importance and is attracting wide attention as an option for implementing green microelectronics. We achieve temperature sensing and energy harvesting using the anomalous Nernst effect (ANE) in $[\text{IrMn/magnetic metal}]_n$ multilayers, which can be used as on-chip temperature sensors and thermoelectric generators. An increase of 103% (1356%) in the voltage (power) generation coefficient is achieved by increasing the number of periods (n) from 1 to 7, due to the enhanced interfacial spin-orbit-coupled scattering. The voltage and power generation coefficients of an optimized $[\text{IrMn/NiFe}]_5$ sample with geometric dimensions of 1800 μm $\times$ 120 μm reach 1.3 $\mu\text{V K}^{-1}$ and 1.7 pW K^{-2}, respectively. Meanwhile, the exchange bias field introduced by Ir-Mn enables an ANE voltage and power output without an external field. Both features can advance the thermopower applications of $[\text{IrMn/magnetic metal}]_n$ multilayers, especially the $[\text{IrMn/NiFe}]_n$ system, for energy-efficient microelectronics.

DOI: 10.1103/PhysRevApplied.17.024075

I. INTRODUCTION

Thermoelectric power generation to recover and reuse waste heat from electronic devices has gained broad attention as a green microelectronic technology. With the development of such applications as the Internet of Things, big data, and artificial intelligence, heat is produced by the Joule mechanism in large amounts by all microelectronic chips, from mobile phones to supercomputers. Energy dissipation in the form of heat has arisen as a non-negligible issue. In the light of the idea of on-chip thermoelectric power generation, spin caloritronics has emerged, which focuses on the concerted interplay of spin, charge, and heat and aims to harvest energy from waste heat in a spintronic manner [1]. Enriched by the discovery of the spin Seebeck effect (SSE) [2,3], spin-dependent Seebeck effect [4,5], spin Nernst effect [6,7], and spin-Peltier effect [8,9], and the revival of interest in the anomalous Nernst effect (ANE) [10–16], spin caloritronics is not only fundamentally interesting but also useful for applications in this sense [12–15].

In this paper, we demonstrate the use of a material system (ferromagnetic-metal/antiferromagnetic-metal periodic multilayers) and its anomalous Nernst effect for on-chip thermoelectric power generation. In the ANE, which is a thermoelectric phenomenon discovered decades ago [17], a longitudinal temperature gradient ∇T produces a transverse electric field $\mathbf{E}_{\text{ANE}}$ in a magnetic conductor when the magnetization $\mathbf{m}$ is perpendicular to ∇T [Fig. 1(b)] [15]. Here, $\mathbf{E}_{\text{ANE}} = Q_s\mu_0(\mathbf{M} \times \nabla T)$, where Q_s is the anomalous Nernst coefficient and μ_0 is the vacuum permeability. This effect came back into the view of the spintronic community due to its entanglement with the spin Seebeck effect in metallic systems [18,19]. Furthermore, it was found thereafter that the ANE has comparable efficiency as a thermopower generator, with values as follows: FePt, 0.68 $\mu\text{V K}^{-1}$; FePd, 0.47 $\mu\text{V K}^{-1}$; $L1_0$-MnGa, -0.35 $\mu\text{V K}^{-1}$; $D0_{22}$-Mn_2Ga, -0.20 $\mu\text{V K}^{-1}$; and Co/Ni, 0.20 $\mu\text{V K}^{-1}$ [16]. These values are similar to their SSE counterpart, approximately 0.5 $\mu\text{V K}^{-1}$, for garnet-ferrite/Pt systems [12]. This old-fashioned phenomenon thus reignited interest in the community.

There are several advantages of ANE-based thermoelectric generators (TEGs) made of the ferromagnetic (FM)/antiferromagnetic (AFM) multilayers proposed here. For an on-chip TEG, a widely proposed technique is based

*wancaihua@iphy.ac.cn
†xfhan@iphy.ac.cn

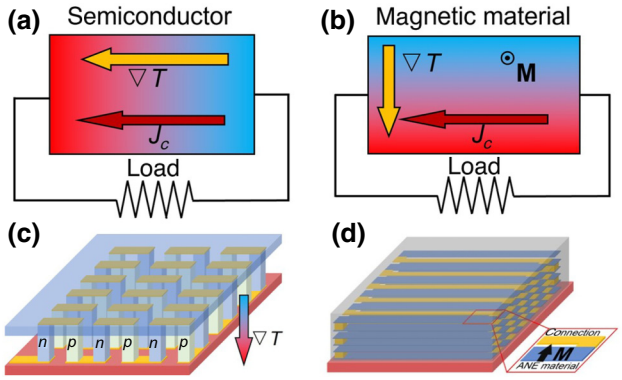

FIG. 1. Schematic images of (a) Seebeck effect (SE) and (b) anomalous Nernst effect. On-chip thermal electric generator using (c) SE and (d) anomalous Nernst effect (ANE). The direction of the temperature gradient, perpendicular to the film normal, is shown in the images.

on the conventional Seebeck effect (SE) [20,21]. This effect generates an electric field parallel to a temperature gradient, i.e., $\mathbf{E}_{\mathrm{SE}} = S_{xx}\nabla T$, where S_{xx} is the Seebeck coefficient [Fig. 1(a)]. Or, for a certain temperature difference $T_{\mathrm{hot}} - T_{\mathrm{cold}}$, the voltage V_{SE} produced in the thermoelectric material becomes $V_{\mathrm{SE}} = S_{xx}(T_{\mathrm{hot}} - T_{\mathrm{cold}})$. A typical SE-based TEG is usually composed of alternately aligned n- and p-type semiconductor pillars with their top electrodes connected in series with the bottom electrodes of adjacent pillars, as shown in Fig. 1(c) [20]. This cascaded structure is complicated to integrate on chips. Furthermore, this SE-based TEG utilizes the temperature difference $T_{\mathrm{hot}} - T_{\mathrm{cold}}$ instead of ∇T along the film normal to harvest energy. An increase in the Seebeck output can be achieved only by two-dimensional expansion of the semiconductor-pillar array. The above constraints on SE TEGs originate from the collinear configuration of the Seebeck voltage and the temperature gradient. In contrast, these constraints can be released for ANE-based TEGs, since the ANE voltage is produced transverse to the temperature gradient ∇T. Compared with SE TEGs, ANE TEGs rely only on a planar connection between magnetic strips, as shown in Fig. 1(d), which is easy to pattern and fabricate. The ANE voltage can be further improved by stacking strip arrays in the depth direction, since each magnetic strip has a much smaller thickness (approximately 40 nm) than the region where ∇T can be built up [22].

On the other hand, the SE normally provides a much higher thermoelectric efficiency than the ANE does for the same material. Therefore, driven by the merits of the ANE over the SE, great efforts have been devoted to enlarging the anomalous Nernst coefficient by material engineering. Although the microscopic picture of the ANE is not fully understood [11,23,24], there exists a view that the ANE has strong correlations with the spin-dependent Seebeck effect and the spin-orbit-coupling (SOC) effect [25,26]. In detail, via the spin-dependent Seebeck effect, a temperature gradient imposed on a ferromagnetic conductor drives a longitudinal pure spin current, which is then deflected into the transverse direction by spin-orbit-coupled scattering and results in an ANE voltage. Following this interpretation, a large ANE can be obtained in diluted magnetic semiconductors, whose Seebeck coefficients are huge compared with metallic systems [11]. For room-temperature applications, however, metallic systems are more favorable. In this case, some alloys and compounds with a large SOC strength such as $L1_0$-ordered Fe-Pt and Mn-Ga alloys have been reported to exhibit high ANE coefficients [14]. Besides the bulk SOC, the interfacial SOC has also been utilized to enhance the ANE, such as in $[\mathrm{Fe/Pt}]_n$, $[\mathrm{Co/Pt}]_n$, and $[\mathrm{Ni/Pt}]_n$ multilayers [23,26,27].

According to the relation between $\mathbf{E}_{\mathrm{ANE}}$ and ∇T, there are two popular setups for characterizing the ANE, one with an in-plane $\nabla_x T$ and an out-of-plane M_z and the other with an out-of-plane $\nabla_z T$ and an in-plane M_x. Many magnetic materials with perpendicular magnetic anisotropy have been studied following the first setup [13,23,25,28]. However, on-chip ANE TEGs ought to work with an out-of-plane $\nabla_z T$, which makes the second setup more realistic in this application scenario. Besides, to fulfill the requirements of the second setup, $\mathbf{M}$ in a magnetic strip should be perpendicular to the stripe orientation, along which the ANE voltage is picked up [see the inset of Fig. 1(d)]. This geometry requires an external magnetic field or a strong magnetocrystalline anisotropy to align the magnetization along the short axis and overcome the shape anisotropy of the magnetic stripes. Sakuraba *et al.* [14] achieved a field-free ANE with an out-of-plane $\nabla_z T$ in epitaxial $L1_0$-ordered MnGa and FePt monolayers, using the uniaxial magnetic anisotropy of a single-crystalline magnet. For polycrystalline films deposited by sputtering, however, their anisotropy is easily dominated by the shape anisotropy, especially for ANE-TEG stacks with a high aspect ratio.

Antiferromagnetic metals such as PtMn and IrMn have both a large spin Hall angle (or strong SOC) and the capability to induce exchange coupling [29–31]. Making full use of the advantages of antiferromagnetic metals, we show here that $[\mathrm{AFM/FM}]_n$ multilayers can simultaneously (1) enhance the SOC-dependent interfacial scattering to improve the ANE coefficient and (2) provide an exchange bias to conquer the shape anisotropy; the results may shed light on high-efficiency and field-free on-chip ANE-TEG devices.

II. EXPERIMENTS

On the basis of the evidence of its considerable spin Hall angle, IrMn is chosen as the antiferromagnetic layer to enhance the interfacial SOC scattering.

Besides, Ir-Mn has been widely used in magnetic random-access memories and magnetic-tunnel-junction sensors, which guarantees its compatibility with current spintronic industrial processes. Stacks with compositions Ta(3 nm)/[IrMn(5 nm)/Co(1.1 nm)]$_n$/IrMn(5 nm)/Ta(3 nm) (with $n = 1$, 3, 5, and 7) and Ta(3 nm)/[IrMn(5 nm)/NiFe or CoFeB(2 nm)]$_5$/IrMn(5 nm)/Ta(3 nm) are deposited with AJA-A320 magnetron sputtering systems (here, IrMn, NiFe, and CoFeB are short for $Ir_{20}Mn_{80}$, $Ni_{80}Fe_{20}$, and $Co_{20}Fe_{60}B_{20}$, respectively). The deposited films are then annealed at 250 °C for 0.5 h in a vacuum chamber in a 0.78-T in-plane field to induce exchange bias. Afterwards, the films are patterned into ANE devices, as sketched in Fig. 2(a). A bar made of [IrMn/ferromagnetic]$_n$ multilayers with dimensions of 1800 μm × 120 μm is used to detect the ANE voltage. A gold bar (10 nm) on top of a SiO_2 insulating spacer (85 nm) is used to heat the samples and provide $\nabla_z T$. A magnetic field is applied transverse to the sample bar to manipulate the magnetization of the multilayer devices. A Keithley 2400 instrument is used to provide a heating current, and a Keithley 2182 instrument is applied to pick up the ANE voltage (V_{ANE}). All the measurements are conducted at 300 K in a physical-property measurement system (Quantum Design-9T) or a three-dimensional magnetic field probe station (East Changing Technologies, China).

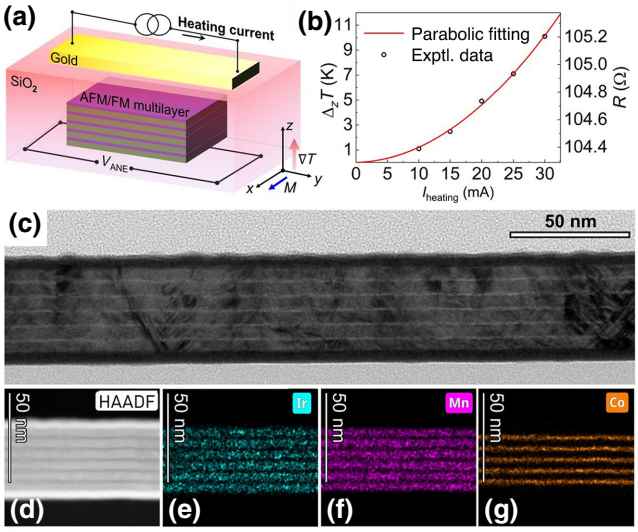

FIG. 2. (a) Schematic illustration of an ANE device with a z-directional temperature difference. When $\nabla_z T$ is produced by the heating current, an anomalous Nernst voltage is then generated along the y axis. (b) Temperature rise along the film normal as a function of heating current. (c) Cross-sectional TEM image of the [IrMn/Co]$_5$ sample, and (d)–(g) HAADF and elemental mapping of the sample obtained in scanning-transmission-electron-microscope mode.

III. RESULTS AND DISCUSSION

A clear multilayer structure is shown by a cross-sectional transmission-electron-microscope (TEM) image of a Ta/[IrMn/Co]$_5$/IrMn/Ta sample, as shown in Fig. 2(c). A high-angle-annular-dark-field (HAADF) image and corresponding elemental mapping, as shown in Figs. 2(d)–2(g), also indicate that the interfaces between the Ir-Mn and the Co are sharp and flat.

Figure 2(a) shows the setup used to measure the ANE. A current flowing through the gold bar heats the sample and produces a z-directional temperature difference ($\Delta_z T$), a magnetic field applied along the x direction changes the magnetization of the multilayer, and V_{ANE} is detected along the y axis. We deduce the value of $\Delta_z T$ caused by the heating current via monitoring the resistance change of the heating electrode while applying the heating current. The resistance change is then compared with the R-T relation of the heating electrode to obtain the temperature rise. The extrapolated $\Delta_z T$-$I_{heating}$ curve can be fitted well by a parabolic function with negligible intercept, as shown in Fig. 2(b).

The dependence of V_{ANE} on the applied field (H_x) for the [IrMn/Co]$_n$ samples with n=1, 3, 5, and 7 shows a similar pattern to their M-H loops (Fig. 3). A larger heating current results in a higher V_{ANE} amplitude. The polarity of the heating current, positive or negative, does not influence the magnitude of V_{ANE} [32]. These features have the characteristics of the ANE. Except for the $n = 1$ sample, the samples are all exchange-biased to a positive field above 1 kOe. The exchange bias field gradually increases with an increase in n. Although the different Co layers are separated by the IrMn layers, they are ferromagnetically coupled. With an increase in the number of interfaces between the Co layers and Ir-Mn layers, it seems natural that the exchange bias should increase, since more interfacial Co spins in the system become fixed.

The field dependence of V_{ANE} obtained also exhibits a significant exchange-bias effect for $n = 3$, 5, and 7 after compensation of the shape anisotropy. A bias field above 1 kOe is retained for the patterned devices, which endows these devices with excellent resistance against high-temperature disturbance. At a heating current of 30 mA, V_{ANE} can still maintain 78%–90% of its saturated value at zero field, which supports the possibility of field-free applications of such devices.

Figure 4(a) summarizes the saturated values of V_{ANE} as a function of the z-directional temperature difference ($\Delta_z T$) for different samples. Although we are not able to accurately calculate the z-directional temperature gradient ($\nabla_z T$), the $\Delta_z T$ dependence of V_{ANE} shows excellent linearity and a negligible intercept, which indicates a reliable ANE origin of our data. We then use $V_{ANE} = S_{xy}\,\Delta_z T$ to fit the V_{ANE}-vs-$\Delta_z T$ dependence. Here S_{xy} is the voltage generation coefficient, which is proportional to the anomalous

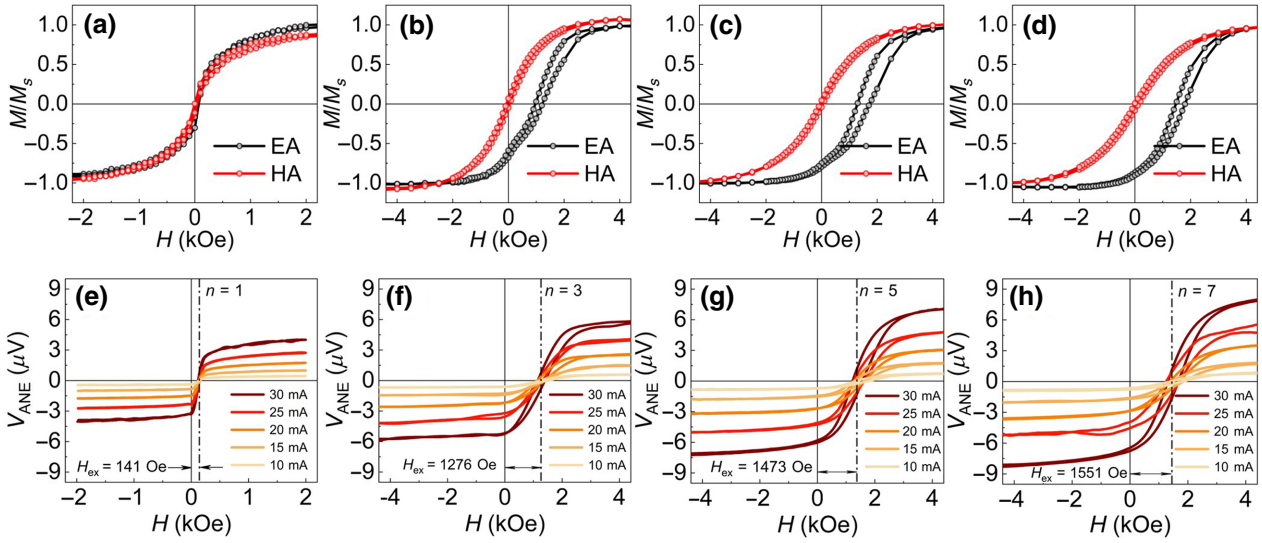

FIG. 3. Magnetization curves [the black curves denote the magnetization curves measured with the magnetic field (H) applied in the easy-axis direction (EA curve) collinear with the exchange bias field (H_{ex}), while the red curves denote the magnetization curves measured with H applied in the hard-axis direction (HA curve) perpendicular to H_{ex}] and magnetic field dependence of the anomalous Nernst voltage (V_{ANE}) for $[\text{Ir-Mn/Co}]_n$ samples with (a),(e) $n = 1$, (b),(f) $n = 3$, (c),(g) $n = 5$, and (d),(h) n=7 for different heating currents.

Nernst coefficient. It is worth mentioning that it is reasonable to evaluate the performance of an on-chip TGE with S_{xy}, since this parameter directly characterizes the conversion from temperature difference to electricity.

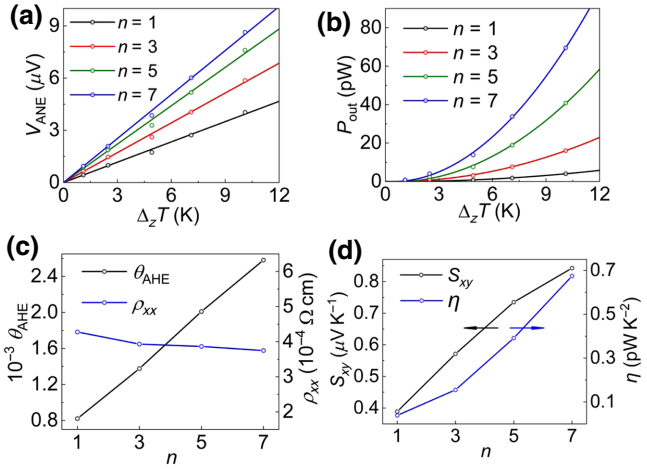

FIG. 4. (a),(b) Dependence of saturated V_{ANE} output and maximum power output (P_{out}) on the z-directional temperature rise ($\Delta_z T$) in $[\text{IrMn/Co}]_n$ samples with $n = 1$, 3, 5, and 7. (c) Dependence of resistivity (ρ_{xx}) and anomalous Hall angle (θ_{AHE}) on n. (d) Summary of ANE coefficient (S_{xy}) and conversion efficiency (η) for the $[\text{IrMn/Co}]_n$ samples. The sensitivity is taken from the slope of a linear fitting of V_{ANE} as a function of $\Delta_z T$, and η is taken from a parabolic fitting of P_{out} as a function of $\Delta_z T$, with $P_{out} = \eta(\Delta_z T)^2$.

Remarkably, S_{xy} shows a noticeable growth with the number of stacking periods n. S_{xy} increases by 103% from $n = 1$ to $n = 7$, as shown in Fig. 4(d). We perform finite-element modeling to investigate the temperature profile of the system [32,33]. The results show that (1) nearly the same temperature gradient occurs in the multilayers if we suppose a similar thermal conductivity for the multilayers, and (2) the Si/SiO_2 substrates can safely function as heat sinks. In this case, the remarkably enlarged S_{xy} indicates the effectiveness of the multilayer structure in enhancing the ANE voltage. When these multilayer devices are applied as thermopower generators, the maximum output power is given by $P_{out} = V_{ANE}^2/4R$, where R is the resistance of the multilayer device. The dependence of P_{out} on $\Delta_z T$ is shown in Fig. 4(b); it looks parabolic and can be fitted well using $P_{out} = \eta(\Delta_z T)^2$. This parabolic dependence is reasonable, since V_{ANE} scales linearly with $\Delta_z T$. The power factor η also qualifies the effectiveness of the ANE in converting thermal energy into electricity. Figure 4(d) shows that η increases by 1356% from $n = 1$ to $n = 7$, demonstrating that the multiperiod stacking strategy is very effective for improving the energy conversion efficiency of ANE-based TEGs.

The enhanced anomalous Nernst voltages in the $[\text{FM/IrMn}]_n$ multilayers have two origins in principle: (1) the bulk ANE effect in the magnetic layers and (2) the increased number of interfaces with strong spin-orbit coupling. Fang *et al.* [23] have presented a picture of the ANE: a spin current produced in a ferromagnetic layer driven by a temperature gradient is deflected transversely via the inverse spin Hall effect, which leads to the ANE.

For bulk FM layers and corresponding $[FM/IrMn]_n$ multilayers, since they share the same FM layers, with the same spin-dependent Seebeck coefficient, the spin currents produced in them should be close to each other. Then, the final ANE voltage should depend strongly on the inverse spin Hall angle of the system. For the multilayers, the spin current can also be converted into an electric current in the IrMn layers, with a much higher spin Hall angle. It is thus no wonder that these multilayers can have a higher ANE coefficient. Certainly, the larger stacking number also results in a larger volume of magnetic layers, which is also an factor that increases the ANE voltage [32]. In order to disentangle the above two factors, we also fabricate thermoelectric devices with the same total thickness of magnetic layers but with different stacking numbers [32]. The measured S_{xy} values are then normalized by the $M_s V$ values. In this case, the normalized S_{xy} still shows a 262% increase from $n = 1$ to 5, which indicates that the magnetic metal/antiferromagnetic metal interfaces alone are effective in improving the ANE coefficient.

This interfacial scattering mechanism can be further amplified in a multilayer or superlattice structure by increasing the number of interfaces [26,27]. Here, to qualify the interfacial SOC scattering, we also measure the anomalous Hall angle (θ_{AHE}) of the multilayers, as shown in Fig. 4(c). θ_{AHE} increases by 315% when n is increased, indicating enhanced interfacial SOC scattering. It is worth noting that the resistivity (ρ_{xx}) of the multilayers varies much more weakly than θ_{AHE}, showing that the interfaces mainly increase transverse rather than backward scattering. Here, we use only seven periods, due to the increased roughness of the upper layers. As deposition techniques improve, there should be no limitation on the maximum number of periods, which is of benefit for the prospects of this multilayer structure to provide an enhanced ANE.

The influence of magnetic materials on thermoelectric generation is also studied, as shown in Fig. 5. Ferromagnetic materials such as Co, CoFeB, and NiFe have been widely used in the spintronic industry. The magnetization curves [Figs. 5(a) and 5(b)] and the field dependence of V_{ANE} [Figs. 5(c) and 5(d)] indicate that an exchange bias is obtained in the NiFe sample but not in the CoFeB sample. The $\Delta_z T$ dependences of V_{ANE} and P_{out} are shown in Figs. 5(e) and 5(f) and are linear and parabolic, respectively, as with the previous Co samples. A comparison of the final performance is shown in Fig. 5(g). Although Co-Fe-B has overwhelmingly larger values of S_{xy} and η, it fails to show an exchange bias. Instead, the Ni-Fe sample has the optimum comprehensive performance, which is suitable for the coming device applications. Its voltage generation coefficient of 1.3 μV K^{-1} seems considerable when it is compared with the Seebeck coefficients -5.1 μV K^{-1} of the metal Pt [34] and -10 μV K^{-1} of $Ni_{80}Fe_{15}$ (5%Mo) [5]. Normally, the ANE coefficient

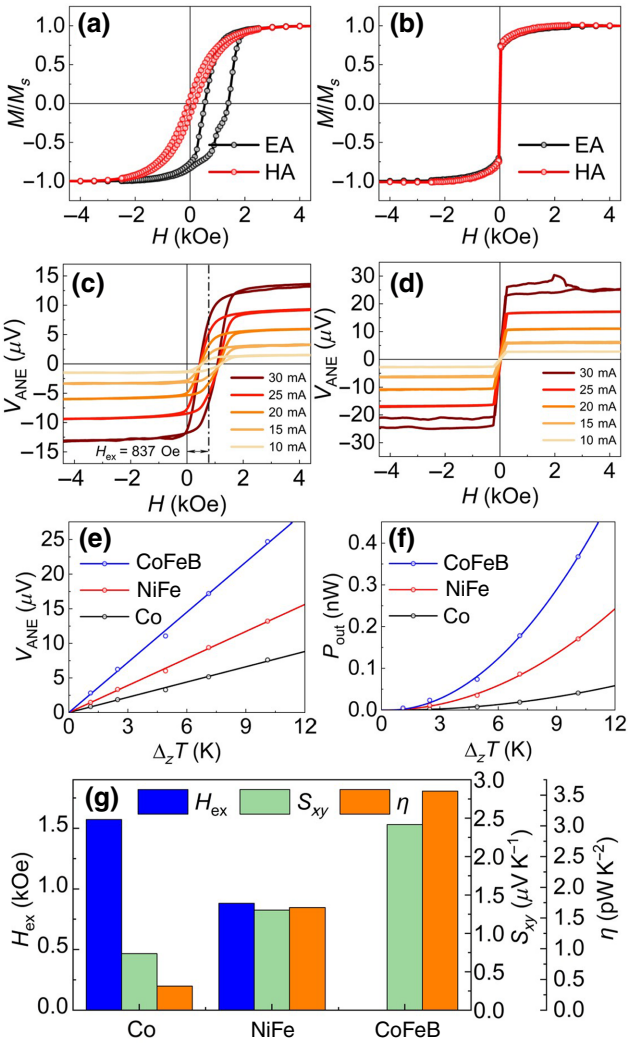

FIG. 5. Magnetization curves [the black curves denote the magnetization curves measured with the magnetic field applied in the EA direction, while the red curves denote the magnetization curves measured with field applied in the HA direction] and magnetic field (H) dependence of V_{ANE} for the (a),(c) $[IrMn/NiFe]_5$ and (b),(d) $[IrMn/CoFeB]_5$ samples. (e),(f) Dependence of the saturated V_{ANE} output and maximum power output (P_{out}) on the z-directional temperature rise ($\Delta_z T$) for the three samples used here. (g) Summary of exchange bias field (H_{ex}), ANE coefficient (S_{xy}), and conversion efficiency (η) for the three samples. The NiFe sample has the optimum performance.

is about 2 orders smaller than the Seebeck counterpart; this is true for many bulk magnets [5,28,35]. Moreover, the power factor η of $[IrMn/NiFe]_5$ reaches 1.7 pW K^{-2}, 1 order of magnitude larger than that of spin-Seebeck thermopower devices [12].

Noticeably, because $E_{ANE} \propto M_x \Delta_z T$, it is straightforward to increase $V_{ANE} = E_{ANE} l$ by increasing the length (l) of the ANE stripes. Since V_{ANE} and R both vary linearly with l and $P_{out} = V_{ANE}^2/4R$, P_{out} also increases linearly with l. Thus, both the temperature-sensing (V_{ANE}) and the

thermopower-generation (P_{out}) performance of an ANE device can be easily doubled by simply doubling its length, which is an advantageous optimization strategy for ANE devices.

In our case, the ANE-TEG devices are 1800 (120) μm in length (width). For the $[IrMn/NiFe]_5$ device, with $R = 250$ Ω, V_{ANE} and P_{out} are thus 13.1 μV and 0.2 nW, respectively, for a $\Delta_z T$ of 10.1 K. As explained above, technically, one can connect hundreds of devices in series or parallel to form an ANE array to amplify the output voltage and power. Following this principle, we indeed pattern three other series-connected devices with 1, 3, and 5 repeating units. As expected, the output V_{ANE} of the latter two devices is 3 times and 5 times, respectively, as large as that of the first device [32].

For a typical CPU with a size of 50 × 50 mm and a working surface temperature of approximately 60 °C [21], we suppose that a 50 mm × 120 μm $[IrMn/NiFe]_5$ strip is used as an ANE unit, and assume that a $\Delta_z T$ of 40 K is maintained over a depth of 1 μm (the typical height of a semiconductor pillar in an on-chip SE TEG). A series connection of 250 units in each layer with 10 layers of stacking can be achieved. In this design, the output V_{ANE} and P_{out} can ideally reach approximately 3.6 V and approximately 13.9 μW, respectively, which are larger than the output power (5 μW at $\Delta_z T = 40$ K) of a SE TEG proposed earlier [36]. This large voltage can be easily measured, and, at the same time, the output electricity, in the order of 10 μW, can easily power microwave devices [37]. In this regard, the proposed ANE-TEG device can be applied as a self-sustaining CPU-temperature monitor and, at the same time, a thermoelectric power generator to power a microwave reporter.

IV. CONCLUSION

$[IrMn/ferromagnetic\ metal]_n$ periodic multilayers are optimized to enhance the anomalous Nernst effect by strengthening the interfacial spin-orbit-coupling scattering. The ANE coefficient (energy conversion efficiency) is increased by 103% (1356%) on going from $n = 1$ to $n = 7$. When we compare different ferromagnetic candidates, we find that the $[IrMn/NiFe]_5$ sample shows balanced performance in terms of exchange bias, output power, and anomalous Nernst voltage. The voltage generation coefficient and power factor for the $[IrMn/NiFe]_5$ sample reach 1.3 $\mu V\ K^{-1}$ and 1.7 $pW\ K^{-2}$, respectively. This paper shows that these $[antiferromagnetic\ film/magnetic\ film]_n$ multilayers can be utilized as practical on-chip ANE-based thermoelectric generators with an energy conversion efficiency comparable with their Seebeck-effect-based counterparts but with better compatibility with CMOS technologies.

ACKNOWLEDGMENTS

The authors appreciate financial support from the National Key Research and Development Program of China (MOST) (Grant No. 2017YFA0206200), the National Natural Science Foundation of China (NSFC) (Grants No. 51831012, No. 11974398, and No. 12061131012), the Beijing Natural Science Foundation (Grant No. Z201100004220006), and the Strategic Priority Research Program (B), the Key Research Program of Frontier Sciences, and the K. C. Wong Education Foundation of the Chinese Academy of Sciences (CAS) (Grants No. XDB33000000, No. QYZDJ-SSW-SLH016, and No. GJTD-2019-14). C. H. Wan appreciates financial support from the Youth Innovation Promotion Association, CAS (2020008).

[1] G. E. Bauer, E. Saitoh, and B. J. Van Wees, Spin caloritronics, Nat. Mater. **11**, 391 (2012).

[2] K. Uchida, J. Xiao, H. Adachi, J. Ohe, S. Takahashi, J. Ieda, T. Ota, Y. Kajiwara, H. Umezawa, and H. Kawai *et al.*, Spin Seebeck insulator, Nat. Mater. **9**, 894 (2010).

[3] K. Uchida, H. Adachi, T. Ota, H. Nakayama, S. Maekawa, and E. Saitoh, Observation of longitudinal spin-Seebeck effect in magnetic insulators, Appl. Phys. Lett. **97**, 172505 (2010).

[4] A. Slachter, F. L. Bakker, J. P. Adam, and B. J. van Wees, Thermally driven spin injection from a ferromagnet into a non-magnetic metal, Nat. Phys. **6**, 879 (2010).

[5] F. K. Dejene, J. Flipse, and B. Van Wees, Spin-dependent Seebeck coefficients of $Ni_{80}Fe_{20}$ and Co in nanopillar spin valves, Phys. Rev. B **86**, 024436 (2012).

[6] T. Seki, Y. Hasegawa, S. Mitani, S. Takahashi, H. Imamura, S. Maekawa, J. Nitta, and K. Takanashi, Giant spin Hall effect in perpendicularly spin-polarized FePt/Au devices, Nat. Mater. **7**, 125 (2008).

[7] T. Seki, I. Sugai, Y. Hasegawa, S. Mitani, and K. Takanashi, Spin Hall effect and Nernst effect in FePt/Au multi-terminal devices with different Au thicknesses, Solid State Commun. **150**, 496 (2010).

[8] J. Flipse, F. Bakker, A. Slachter, F. Dejene, and B. Van Wees, Direct observation of the spin-dependent Peltier effect, Nat. Nanotechnol. **7**, 166 (2012).

[9] S. T. Goennenwein and G. E. Bauer, Electron spins blow hot and cold, Nat. Nanotechnol. **7**, 145 (2012).

[10] Y. Pu, D. Chiba, F. Matsukura, H. Ohno, and J. Shi, Mott Relation for Anomalous Hall and Nernst Effects in $Ga_{1-x}Mn_xAs$ Ferromagnetic Semiconductors, Phys. Rev. Lett. **101**, 117208 (2008).

[11] S. Huang, W. Wang, S. Lee, J. Kwo, and C. Chien, Intrinsic Spin-Dependent Thermal Transport, Phys. Rev. Lett. **107**, 216604 (2011).

[12] K. Uchida, H. Adachi, T. Kikkawa, A. Kirihara, M. Ishida, S. Yorozu, S. Maekawa, and E. Saitoh, Thermoelectric generation based on spin Seebeck effects, Proc. IEEE **104**, 1946 (2016).

[13] W. N. Zhou, K. Yamamoto, A. Miura, R. Iguchi, Y. Miura, K. Uchida, and Y. Sakuraba, Seebeck-driven transverse thermoelectric generation, Nat. Mater. **20**, 463 (2021).

[14] Y. Sakuraba, K. Hasegawa, M. Mizuguchi, T. Kubota, S. Mizukami, T. Miyazaki, and K. Takanashi, Anomalous Nernst effect in $L1_0$-FePt/MnGa thermopiles for new thermoelectric applications, Appl. Phys. Express **6**, 033003 (2013).

[15] M. Mizuguchi and S. Nakatsuji, Energy-harvesting materials based on the anomalous Nernst effect, Sci. Technol. Adv. Mat. **20**, 262 (2019).

[16] K. Hasegawa, M. Mizuguchi, Y. Sakuraba, T. Kamada, T. Kojima, T. Kubota, S. Mizukami, T. Miyazaki, and K. Takanashi, Material dependence of anomalous Nernst effect in perpendicularly magnetized ordered-alloy thin films, Appl. Phys. Lett. **106**, 252405 (2015).

[17] A. W. Smith, The Hall effect and the Nernst effect in magnetic alloys, Phys. Rev. **17**, 23 (1921).

[18] S. Y. Huang, X. Fan, D. Qu, Y. Chen, W. Wang, J. Wu, T. Chen, J. Xiao, and C. Chien, Transport Magnetic Proximity Effects in Platinum, Phys. Rev. Lett. **109**, 107204 (2012).

[19] C. X. Liu, S. Schuwalow, Y. Liu, K. Vilkelis, A. L. R. Manesco, P. Krogstrup, and M. Wimmer, Electronic properties of InAs/EuS/Al hybrid nanowires, Phys. Rev. B **104**, 014516 (2021).

[20] G. B. Abdallah, S. Besbes, H. B. Aissia, and J. Jay, Analysis of the effect of a pulsed heat flux on the performance improvements of a thermoelectric generator, Appl. Therm. Eng. **158**, 113728 (2019).

[21] H. Fahad, M. Hasan, G. D. Li, and M. Hussain, Thermoelectricity from wasted heat of integrated circuits, Appl. Nanosci. **3**, 175 (2013).

[22] M. A. Cabero Z, C. Y. Guo, C. H. Wan, J. F. Hu, S. Liu, M. K. Zhao, L. B. Zhang, Q. M. Song, H. C. Wang, and S. Tu *et al.*, Electron-phonon interaction enables strong thermoelectric Seebeck effect variation in hybrid nanoscale systems, J. Phys. Chem. C **125**, 13167 (2021).

[23] C. Fang, C. H. Wan, Z. H. Yuan, L. Huang, X. Zhang, H. Wu, Q. T. Zhang, and X. F. Han, Scaling relation between anomalous Nernst and Hall effect in $[Pt/Co]_n$ multilayers, Phys. Rev. B **93**, 054420 (2016).

[24] D. Xiao, Y. G. Yao, Z. Fang, and Q. Niu, Berry-Phase Effect in Anomalous Thermoelectric Transport, Phys. Rev. Lett. **97**, 026603 (2006).

[25] A. A. Tulapurkar and Y. Suzuki, Contribution of electron-magnon scattering to the spin-dependent Seebeck effect in a ferromagnet, Solid State Commun. **150**, 466 (2010).

[26] T. Seki, Y. Sakuraba, K. Masuda, A. Miura, M. Tsujikawa, K. Uchida, T. Kubota, Y. Miura, M. Shirai, and K. Takanashi, Enhancement of the anomalous Nernst effect in Ni/Pt superlattices, Phys. Rev. B **103**, L020402 (2021).

[27] K. Uchida, T. Kikkawa, T. Seki, T. Oyake, J. Shiomi, Z. Y. Qiu, K. Takanashi, and E. Saitoh, Enhancement of anomalous Nernst effects in metallic multilayers free from proximity-induced magnetism, Phys. Rev. B **92**, 094414 (2015).

[28] T. C. Chuang, P. L. Su, P. H. Wu, and S. Y. Huang, Enhancement of the anomalous Nernst effect in ferromagnetic thin films, Phys. Rev. B **96**, 174406 (2017).

[29] J. B. S. Mendes, R. O. Cunha, O. A. Santos, P. R. T. Ribeiro, F. L. A. Machado, R. L. Rodríguez Suárez, A. Azevedo, and S. M. Rezende, Large inverse spin Hall effect in the antiferromagnetic metal $Ir_{20}Mn_{80}$, Phys. Rev. B **89**, 140406 (2014).

[30] W. J. Kong, Y. R. Ji, X. Zhang, H. Wu, Q. T. Zhang, Z. H. Yuan, C. H. Wan, X. F. Han, T. Yu, and K. Fukuda *et al.*, Field-free spin Hall effect driven magnetization switching in Pd/Co/IrMn exchange coupling system, Appl. Phys. Lett. **109**, 132402 (2016).

[31] S. Tu, J. F. Hu, G. Q. Yu, H. M. Yu, C. P. Liu, F. Heimbach, X. R. Wang, J. Y. Zhang, Y. G. Zhang, and A. Hamzić *et al.*, Anomalous Nernst effect in $Ir_{22}Mn_{78}/Co_{20}Fe_{60}B_{20}/MgO$ layers with perpendicular magnetic anisotropy, Appl. Phys. Lett. **111**, 222401 (2017).

[32] See Supplemental Material at http://link.aps.org/supplemental/10.1103/PhysRevApplied.17.024075, for heating current polarity dependence of ANE signals, period number dependence of temperature gradient across magnetic multilayers, saturated magnetization of magnetics multilayers, enhancing ANE output by interfacial scattering and demonstration of serially connected devices.

[33] K. D. Lee, D. J. Kim, H. Y. Lee, S. H. Kim, J. H. Lee, K. M. Lee, J. R. Jeong, K. S. Lee, H. S. Song, J. W. Sohn, S. C. Shin, and B. G. Park, Thermoelectric signal enhancement by reconciling the spin Seebeck and anomalous Nernst effects in ferromagnet/non-magnet multilayers, Sci. Rep. **5**, 10249 (2015).

[34] J. P. Moore and R. S. Graves, Absolute Seebeck coefficient of platinum from 80 to 340 K and the thermal and electrical conductivities of lead from 80 to 400 K, J. Appl. Phys. **44**, 1174 (1973).

[35] A. D. Avery, R. Sultan, D. Bassett, D. Wei, and B. L. Zink, Thermopower and resistivity in ferromagnetic thin films near room temperature, Phys. Rev. B **83**, 100401 (2011).

[36] P. Fan, Z. H. Zheng, Z. K. Cai, T. B. Chen, P. J. Liu, X. M. Cai, D. P. Zhang, G. X. Liang, and J. T. Luo, The high performance of a thin film thermoelectric generator with heat flow running parallel to film surface, Appl. Phys. Lett. **102**, 033904 (2013).

[37] R. Ishikawa, T. Yoshida, and K. Honjo, A 2.4 GHz-band enhancement-mode GaAs HEMT rectifier with 19% RF-to-DC efficiency for 1μW input power, 49th European Microwave Conference (EuMC) (2019).